Chapter 7

Shock waves in the solar corona

7.1 Moreton waves and EIT waves

Wave-like fronts were observed in Hα by Moreton & Ramsay (1960). They were interpreted as fast MHD (flare) waves that propagate to the corona, their chromospheric "skirt" being observed in Hα (Uchida 1968, 1974). SOHO EIT observed "EIT waves" in 1997, which brought back the question on solar waves. Later on, wave-like fronts were also detected in soft X-rays, He I, microwaves, etc.

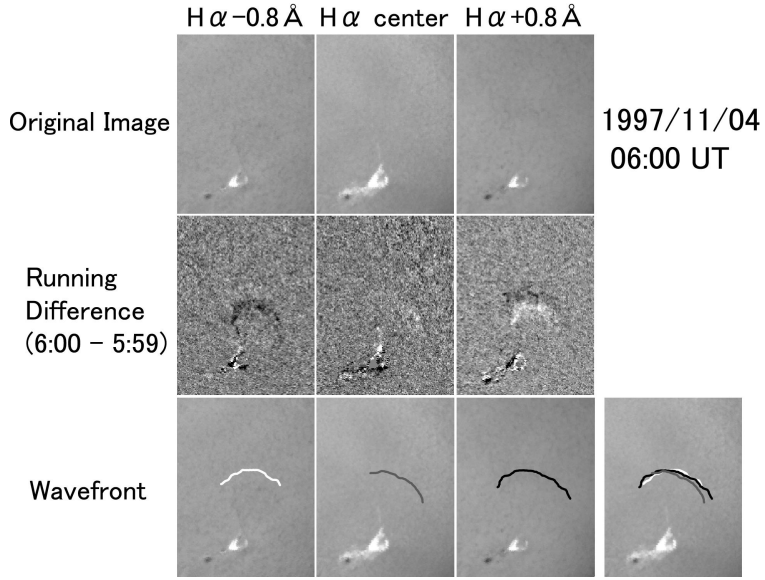

Figure 7.1: Example of a Moreton wave front that is best observed in difference images. The waves sometimes slow down when they encounter other (dense) structures.

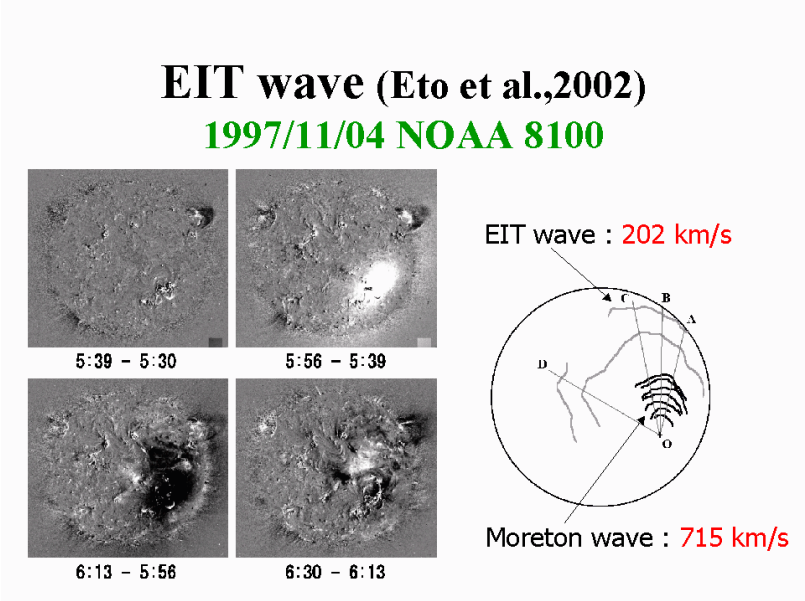

Figure 7.2: Example of a Moreton wave observed together with an EIT wave.

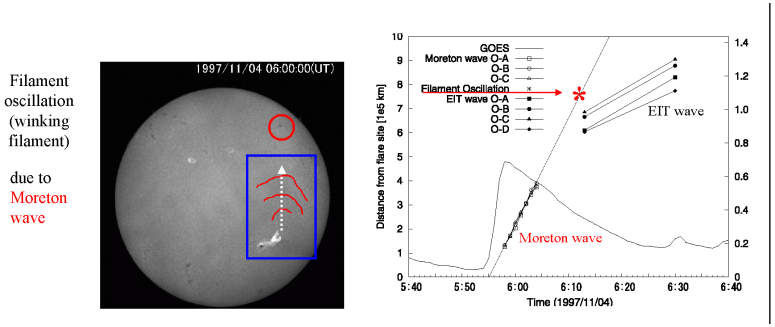

Figure 7.3: The speeds of Moreton waves and EIT waves look different. On the other hand, we do not know where and when EIT waves are formed, and therefore comparisons are difficult. Also instrument time cadence is often insufficient to determine start times for waves.

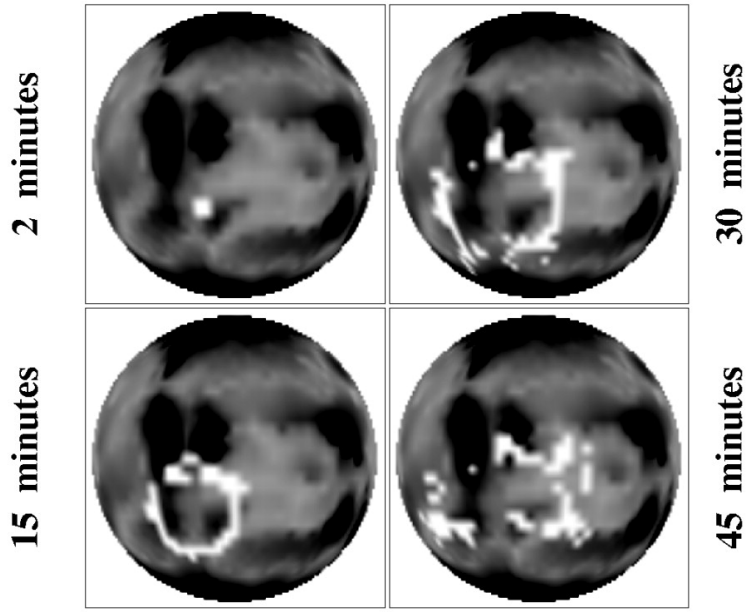

Figure 7.4: Simulation of the April 7 (Wang, ApJ 543, 2000) EUV transient. The wave is deflected away from the large northern hemisphere active region and from the south polar hole, so that the wave front eventually becomes elongated in the direction of the weaker fields to the northwest and southeast of the source. The surface-projected expansion speeds are initially of order 300 km/s but subsequently decrease to less than 200 km/s.

- Uchida et al.: Moreton waves are fast (600 – 1000 km/s) and EIT waves are slow (200 – 350 km/s), so the waves must be different
- Warmuth et al., Pohjolainen et al.: Cases of cospatial Moreton and EIT waves observed, associated with type II bursts
- Wang: Moreton waves can create EIT waves, but simulations do not produce any fast EIT waves or associated type II bursts
- Alternative interpretations for EIT waves: they are signatures of magnetic field evolution during CME lift-off (Delannee, ApJ 2000)
- Or, the waves may be due to Joule heating, resulting from the generation of electric currents (Delannee et al., 2007)
- Or, they are a signature of reconnection between the expanding magnetic cloud (CME) and low-lying fields (Attrill et al., 2007)

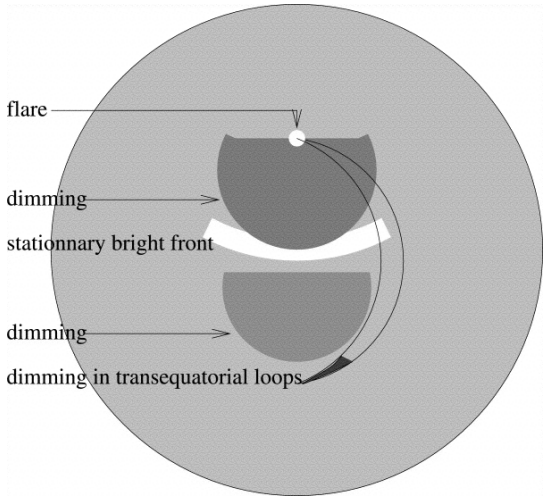

Figure 7.5: Delannee, ApJ 2000: EIT waves are a signature of magnetic field evolution during CME lift-off?

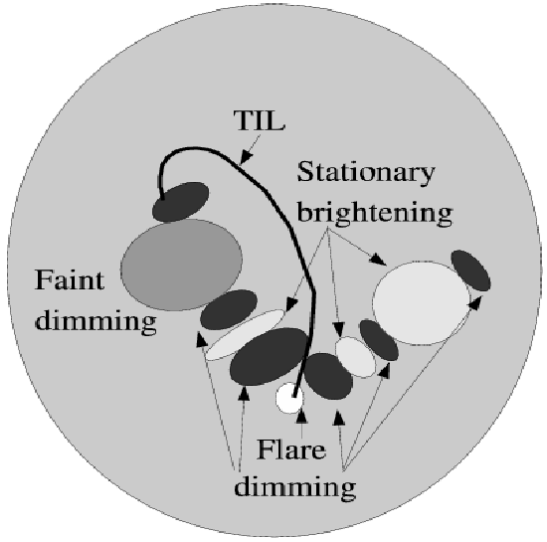

Figure 7.6: EIT and Moreton waves present stationary brightenings - the waves may be due to Joule heating resulting from the generation of electric currents in the neighboring area of the drastic jumps of magnetic connectivity, while the magnetic field lines are opening during a CME (Delannee et al., 2007).

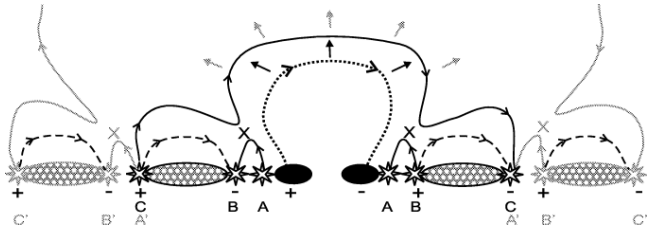

Figure 7.7: Magnetic reconnection model proposed to generate the bright, diffuse coronal "wave" front, with the observed dual brightenings. The expanding CME (dotted line) reconnects with favourably orientated quiet-Sun magnetic loops (dashed lines), displacing the footpoints of the expanding CME (solid line). The crosses mark regions where magnetic reconnection occurs (Attrill et al., 2007).

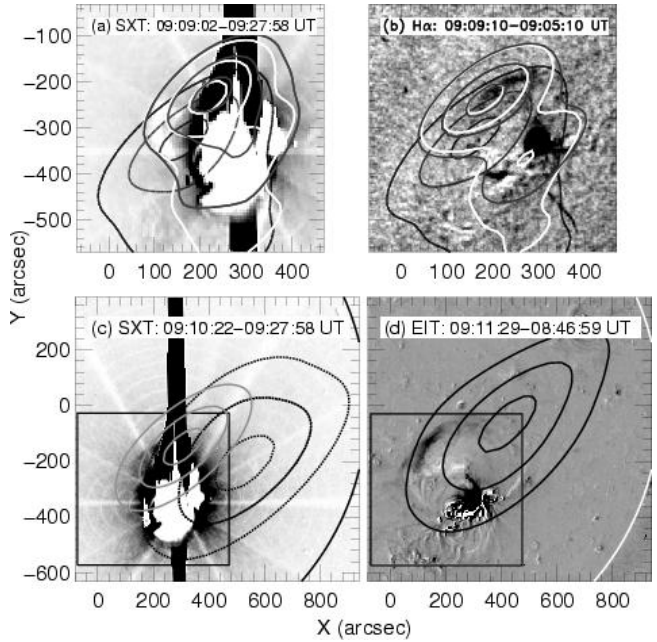

Figure 7.8: Portions of soft X-ray, Hα, and EUV difference images with overplotted Nancay Radioheliograph image contours during the type II burst emission. The image shows how the type II burst emission is located near the soft X-ray, EIT, and Moreton wave fronts. (Khan & Aurass, A&A, 2002).

7.2 Radio type II bursts

Frequency-drifting emission is observed at the fundamental plasma frequency and its harmonics (twice or three times the fundamental frequency).

– Coronal type II bursts are observed at 400 – 15 MHz.
– Interplanetary type II bursts are observed at 14 MHz – 30 kHz.
– Calculated source velocities are ~ 500 – 1000 km/s.

Radio type II emission is created by accelerated particles that produce Langmuir waves, these waves then convert to radio waves. Best continuous accelerator for particles is a shock wave. However, there are several candidates for the sources and origins of shock waves:

- Flare (blast) waves
- Bow shocks ahead of CMEs or fast ejecta
- CME-driven shocks
- Shocks at the flanks of CMEs

Basic shock types that are commonly associated with CMEs are bow shocks and piston-driven shocks. The basic differences can be described with the following cartoons:

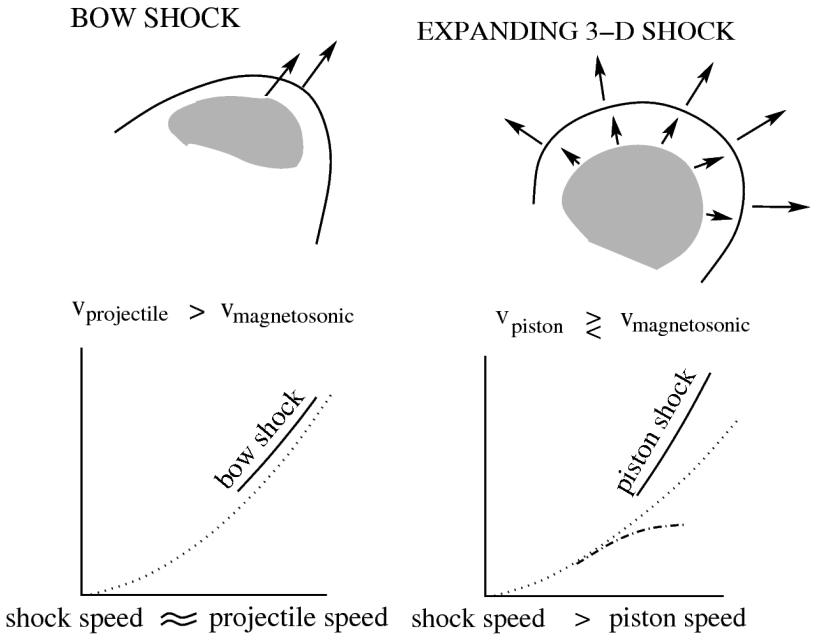

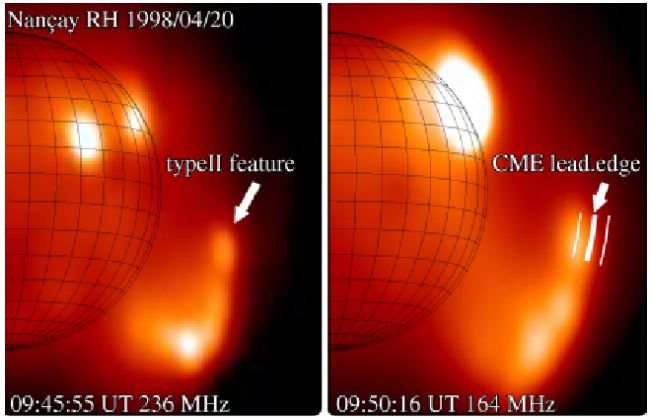

Figure 7.9: Observations of radio type II burst origins: Type II burst driver is the CME bow shock (Maia et al. ApJ, 2000).

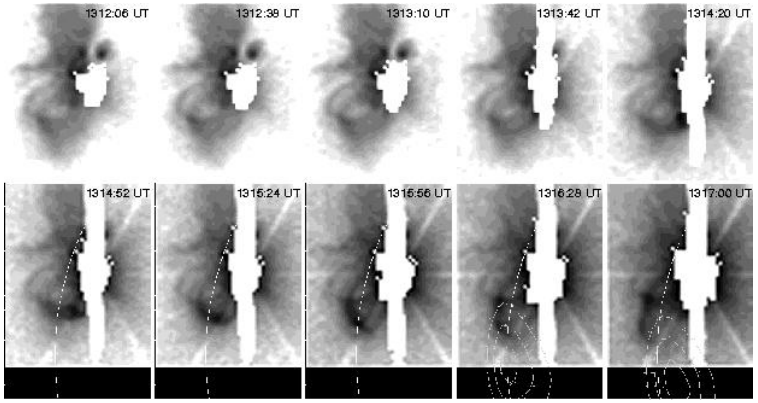

Figure 7.10: Observations of radio type II burst origins: Type II burst driver is a plasmoid (Klein et al., 1999). A sequence of Yohkoh SXT flare-mode, partial frame images of AR 8113 and its surroundings before and at the onset of a type II burst. The first images show diffuse and highly inclined loops extending south-eastward from the inner active region whose emission saturates the detector. In the subsequent images a localized brightening seems to rise along the southern legs of these loops at a projected speed of 770 km s^{-1}. When this blob reaches the loop top near 13:16 UT, the loop expands and seems to disrupt. The first high-frequency signature of the type II burst becomes visible near the time of disruption, and just above the loop top.

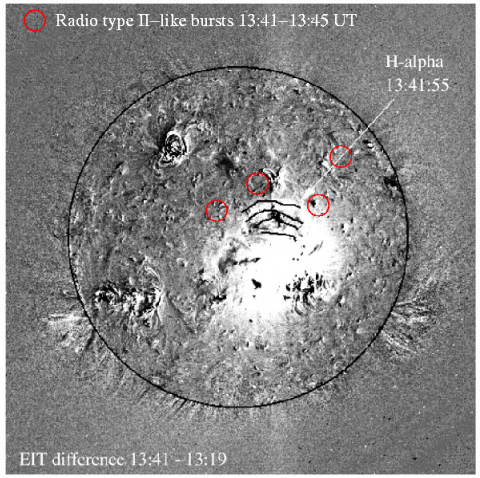

Figure 7.11: Observations of radio type II burst origins: Type II burst driver is the Moreton/EIT wave (Pohjolainen et al. 2001).

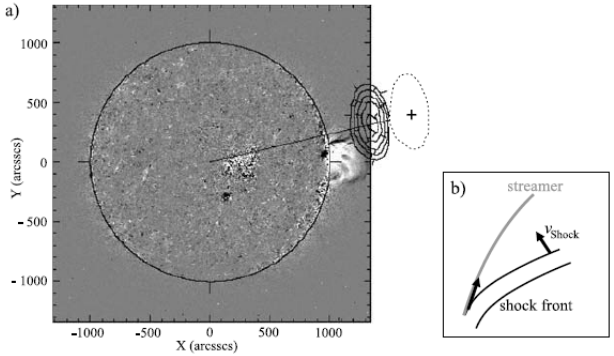

Figure 5 (a) NRH radio source (13:10:07 UT), corresponding to the harmonic band of the 1st type II burst (H1), superposed on the EIT image (13:14:14 UT). The corrected position of the radio source is marked by the cross and dashed curve. (b) Geometry of the shock front and the field line of the streamer; such an interaction between the shock front and the streamer can lead to a significant overestimate of the radio source velocity.

Figure 7.12: Observations of radio type II burst origins: The type II burst is located much higher than the CME front (Magdalenic et al. 2008). Note that the background EIT image was taken at 13:14 UT and the type II burst (contours) was observed at 13:10 UT - and hence the corrected even higher height (center marked with cross) for the type II burst at the time when the EIT image was taken.

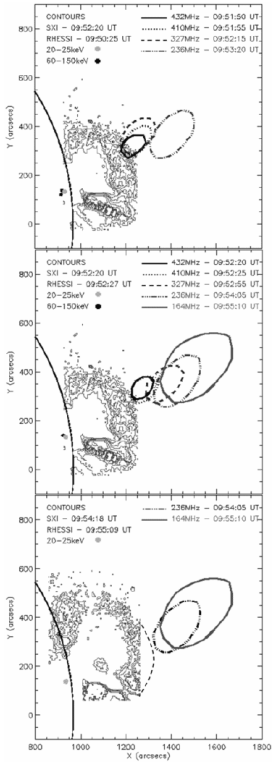

Figure 7.13: Observations of radio type II burst origins: Type II burst driver is the rising SXR loop (Dauphin et al. 2006).

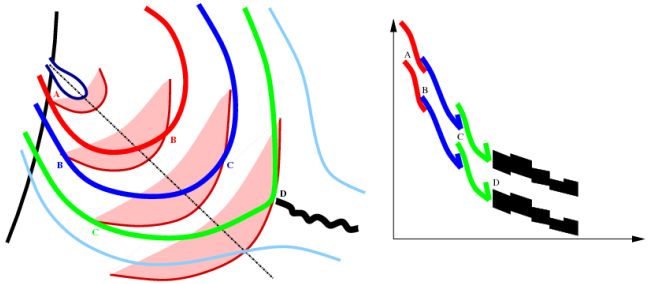

Figure 7.14: Observations of radio type II burst origins: Fragmented type II bursts are observed when shock wave passes through high-density loops (Pohjolainen, Pomoell & Vainio, 2008).

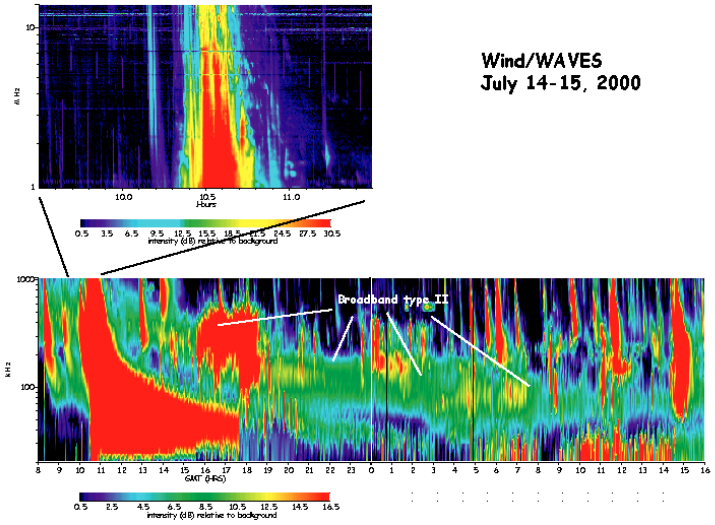

Figure 7.15: Wind WAVES dynamic radio spectrum at two frequency bands, 1–14 MHz (top) and 20 kHz – 1 MHz (bottom). A propagating (interplanetary, IP) shock is visible at decameter - hectometer waves. Plasma frequency near L1 is 30 – 50 kHz. If electron density is dropping as $\sim 1/r^2$, the speed of the shock driver is about 2400 km/s.

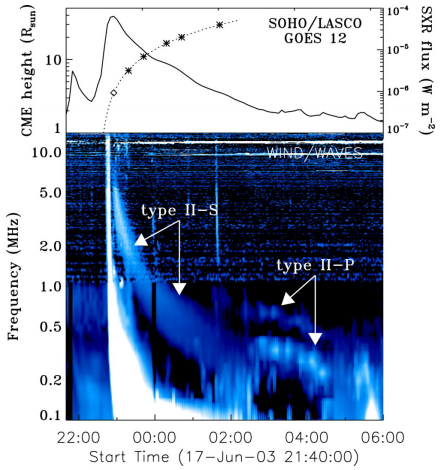

Figure 7.16: But, radio emission at low frequencies is not always plasma emission. Bastian, 2008: plasma (II-P) vs. synchrotron (II-S) emission in IP space.

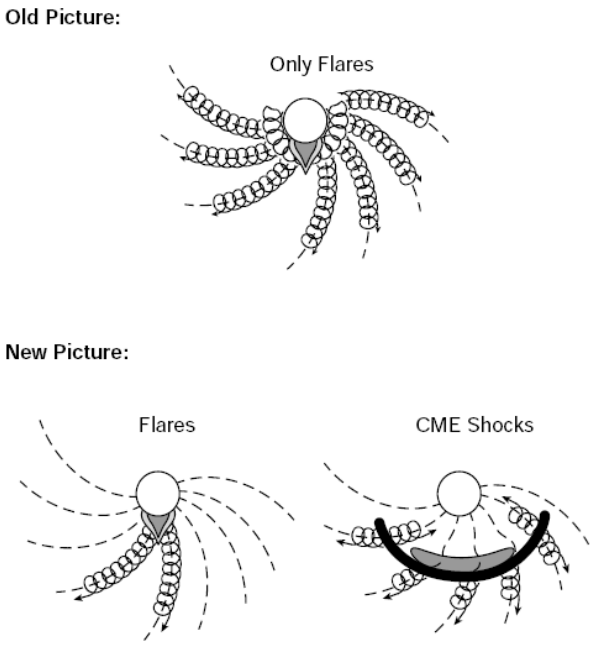

Figure 7.17: Gradual/impulsive SEP paradigm: are impulsive SEP events flare-accelerated and gradual SEP events CME-accelerated? (Reames, Space Science Reviews, 1999).

7.3 Solar energetic particles

For solar energetic particle (**SEP**) events, onset time = start of intensity rise at counting detector; injection time = start of acceleration near Sun; travel time = from injection to onset. You need to correct the times for 8 minutes when compared to electromagnetic emission.

For determining travel times, the methods are
- fixed path length method, assuming that the travel path is 1.2 AU
- velocity dispersion analysis (VDA), based on the fact that particles with higher energies arrive earlier and you can determine one path length and injection time for all energies.

SEP events can be divided into two classes, impulsive and gradual events.

Impulsive events are usually relatively low-intensity and short-duration (from hours to days) events. They are associated with short-duration soft X-ray emission, have high electron to proton intensity ratio and enhanced abundances of heavy elements. There is an association with flare acceleration processes and typical maximum particle energies in impulsive events are ~10 MeV per nucleon, the events are usually observable only if the accompanying flare occurs close to the nominal root (at ~W60) of the interplanetary (IP) magnetic field lines connected to the observer. The particles in these events are generally believed to be accelerated in impulsive solar flares.

In contrast, gradual SEP events have higher particle intensities and power-law energy spectra extending to higher energies (in the case of protons beyond 1 GeV in extreme cases). The SEP events have long durations (days to weeks), and they are associated with long-duration soft X-ray emission and with interplanetary shocks driven by CMEs. The electron to proton ratios are smaller and on average elemental abundances and ionic charge states are in consistency with solar coronal abundances and temperatures.

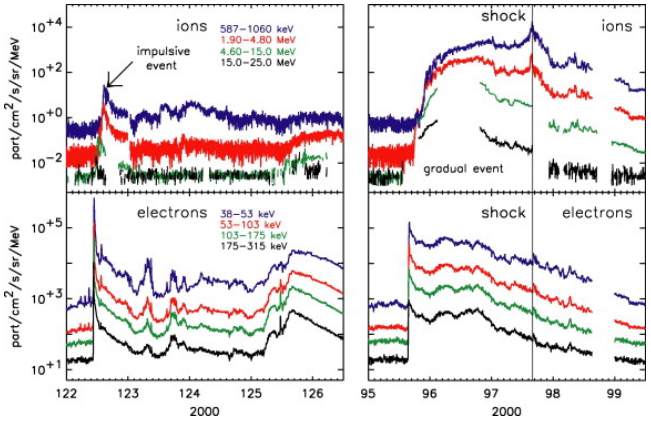

Figure 7.18: From: Lario D., Advances in Space Research, Vol 36, Issue 12, 2005

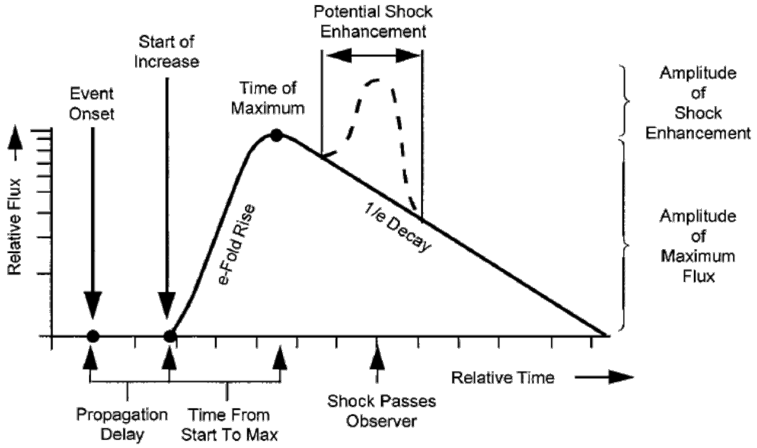

Figure 7.19: From: From: http://dev.sepem.oma.be/help/sep_intro.html

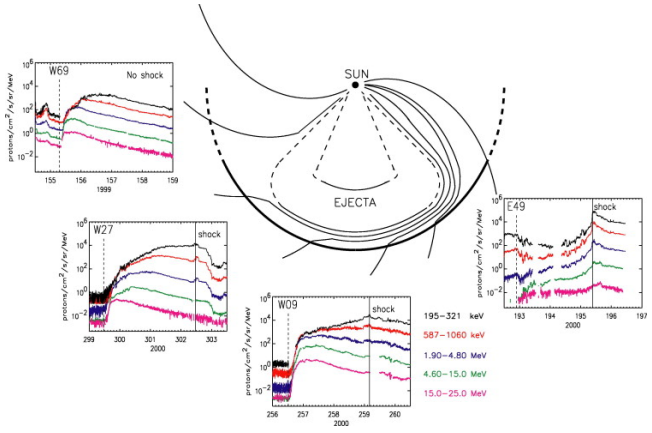

Figure 7.20: From: Lario D., Advances in Space Research, Vol 36, Issue 12, 2005

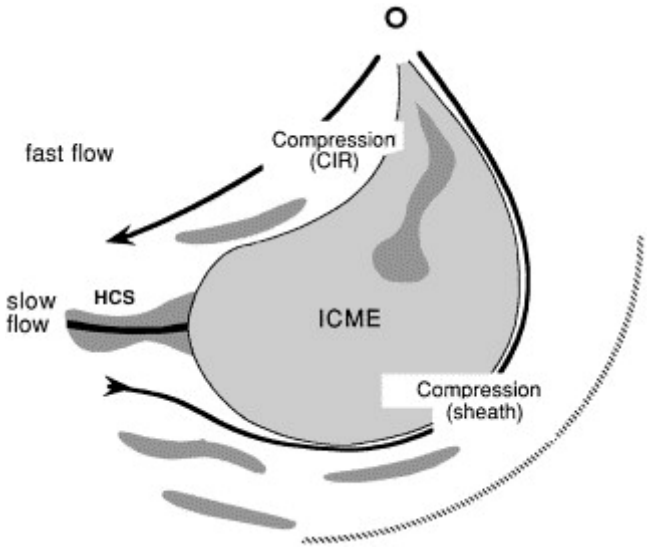

Figure 7.21: Interplanetary CME (ICME) and corotating interaction region (CIR). From: Crooker N., Journal of Atmospheric and Solar-Terrestrial Physics, Volume 62, Issue 12, August 2000

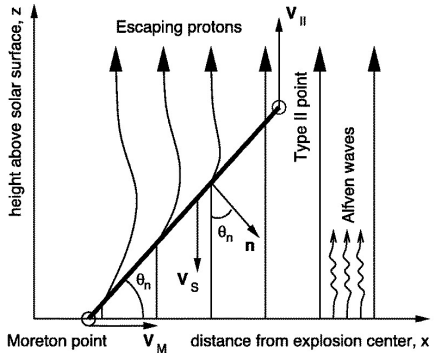

Figure 7.22: Simplified model of the acceleration region. V_M is the Moreton wave speed, θ_n is the (constant) angle between the shock normal n and the magnetic field, V_{II} is the vertical speed deduced from the metric type II drift rate, and $V_S = V_M \tan\theta_n$ is the shock speed projected along the field lines (Vainio & Khan, ApJ 2004).

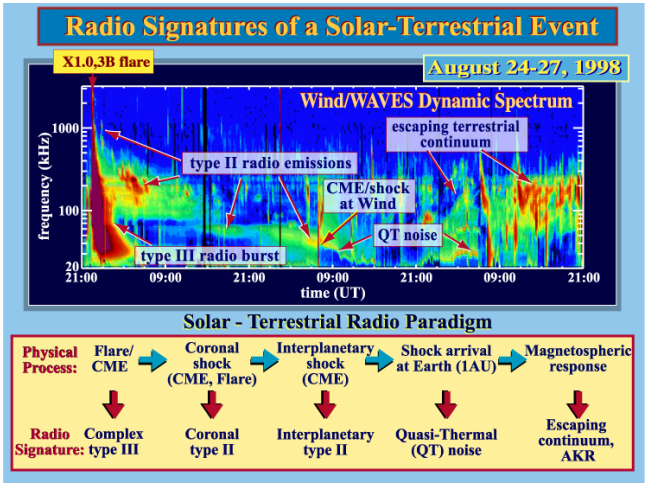

Figure 7.23: From: From: http://swaves.gsfc.nasa.gov/content_images/swavesf1.png